Ouyang *et al. Chem. Synth.* **2025**, *5*, 1
DOI: 10.20517/cs.2024.05

Chemical Synthesis

Research Article

Open Access

Synthesis of metal-phenanthroline-modified hypercrosslinked polymer for enhanced CO_2 capture and conversion via chemical and photocatalytic methods under ambient conditions

Huang Ouyang[1,#], Mengjie Peng[1,#], Kunpeng Song[2], Shengyao Wang[3], Hui Gao[1], Bien Tan[1,*]

[1]Key Laboratory of Material Chemistry for Energy Conversion and Storage, Ministry of Education, Hubei Key Laboratory of Material Chemistry and Service Failure, School of Chemistry and Chemical Engineering, Huazhong University of Science and Technology, Wuhan 430074, Hubei, China.
[2]College of Chemistry and Chemical Engineering, China West Normal University, Nanchong 637009, Sichuan, China.
[3]College of Science, Huazhong Agricultural University, Wuhan 430070, Hubei, China.
[#]Authors contributed equally.

[*]**Correspondence to:** Prof. Bien Tan, Key Laboratory of Material Chemistry for Energy Conversion and Storage, Ministry of Education, Hubei Key Laboratory of Material Chemistry and Service Failure, School of Chemistry and Chemical Engineering, Huazhong University of Science and Technology, Luoyu Road No. 1037, Wuhan 430074, Hubei, China. E-mail: bien.tan@mail.hust.edu.cn

How to cite this article: Ouyang, H.; Peng, M.; Song, K.; Wang, S.; Gao, H.; Tan, B. Synthesis of metal-phenanthroline-modified hypercrosslinked polymer for enhanced CO_2 capture and conversion via chemical and photocatalytic methods under ambient conditions. *Chem. Synth.* **2025**, *5*, 1. https://dx.doi.org/10.20517/cs.2024.05

Received: 14 Jan 2024 **First Decision:** 8 Apr 2024 **Revised:** 7 May 2024 **Accepted:** 16 May 2024 **Published:** 2 Sep 2024

Academic Editor: Feng Shi **Copy Editor:** Pei-Yun Wang **Production Editor:** Pei-Yun Wang

Abstract

Catalytic conversion of CO_2 into valuable chemicals is a promising approach to mitigate the greenhouse effect and alleviate energy shortages. Hypercrosslinked polymers (HCPs) offer a scalable and stable platform for this conversion, but they often suffer from low CO_2 adsorption and activation capabilities, necessitating high temperatures and pressures for effectiveness. To overcome these limitations, nitrogen-based CO_2-philic active sites have been integrated into the structure of HCPs, enhancing CO_2 attraction and leading to superior adsorption performance. The incorporation of cobalt ions further bolsters CO_2 affinity, with HCP-PNTL-Co-B achieving the highest observed adsorption heat of 33.0 kJ·mol^{-1} alongside a substantial 2.0 mmol·g^{-1} CO_2 uptake. These modified HCPs exhibit higher yields and reaction rates in cycloaddition reactions with cocatalyst tetrabutylammonium bromide at room temperature and atmospheric pressure, while HCP-1,10-phenanthroline (PNTL)-Co-B demonstrates a higher CO production rate (2,173 μmol·g^{-1}·h^{-1}) and selectivity (84%) in photocatalytic reduction reaction. This research has successfully achieved outstanding carbon dioxide capture and conversion performance

© The Author(s) 2024. **Open Access** This article is licensed under a Creative Commons Attribution 4.0 International License (https://creativecommons.org/licenses/by/4.0/), which permits unrestricted use, sharing, adaptation, distribution and reproduction in any medium or format, for any purpose, even commercially, as long as you give appropriate credit to the original author(s) and the source, provide a link to the Creative Commons license, and indicate if changes were made.

at room temperature and atmospheric pressure by introducing CO_2-philic active sites and cobalt ions into HCPs *via* facile one-step polymerization. This study provides a new method to design highly efficient organic catalysts for CO_2 conversion.

Keywords: Hypercrosslinked polymers, N heteroatoms, CO_2 cycloaddition, CO_2 photoreduction

INTRODUCTION

The transformation of CO_2 into value-added chemicals offers a dual benefit: it reduces greenhouse gas emissions and recycles carbon resources[1-6]. The domain of CO_2 catalytic conversion has seen the emergence of numerous homogeneous and heterogeneous catalysts[7-11]. Heterogeneous catalysts, including carbon-based materials[12,13], silica[14], metal-organic frameworks (MOFs)[15-17], covalent organic frameworks (COFs)[18,19], and porous organic frameworks (POPs)[20-24], are preferred over their homogeneous counterparts due to their ease of separation, purification, and recyclability. Hypercrosslinked polymers (HCPs), as a subcategory of porous organic polymers, are particularly notable for their high surface area, diverse porosity, affordability, facile functionalization, and robust stability[25-31]. Moreover, HCPs are adept at incorporating catalytic sites, facilitating the creation of multiphase catalytic systems, which positions them as strong candidates for CO_2 conversion applications[32-39].

At mild conditions, the effectiveness of CO_2 conversion is closely tied to the material's CO_2 capture aptitude, with materials exhibiting low adsorption capacities facing limitations due to reduced CO_2 concentrations at catalytic sites[40-42]. Unfortunately, most metal-based HCPs reported to date possess suboptimal CO_2 adsorption capabilities, leading to inefficient utilization of CO_2 under ambient conditions[30,32,37,43]. Beyond merely enhancing the CO_2 adsorption capacity to improve conversion[32,44,45], scant research addresses the interaction between CO_2 and the catalytic material. Integrating CO_2-philic sites, such as nitrogen atoms or nitrogen-functional groups, can bolster the adsorption force for CO_2, amplify adsorption capacity, and concentrate CO_2 around catalytic sites[46-49]. This process not only increases the concentration of CO_2 but also activates the inert CO_2 molecules adsorbed on the surface, thereby improving the conversion efficiency. Nonetheless, the post-functionalization approach for introducing CO_2-philic sites is often labor-intensive and may compromise the integrity of the porous structures of HCPs. It also suffers from the uneven distribution of CO_2-philic sites[50-52]. Alternatively, synthesizing HCPs through hypercrosslinking polymerization with monomers already containing CO_2-philic sites presents a solution, potentially enabling effective CO_2 conversion in ambient conditions.

Motivated by the need to improve interactions with CO_2 and stabilize metal ion catalytic sites, we utilized 1,10-phenanthroline (PNTL), a nitrogen-rich ligand known for its ability to enhance the binding with acidic CO_2 molecules and coordinate with metal ions[53]. We synthesized PNTL-based HCPs through the Friedel-Crafts alkylation, employing derivatives of PNTL as functional monomers [Scheme 1]. This approach strategically increased the nitrogen content within the HCP framework, circumventing the issues of inhomogeneous CO_2-philic site distribution often encountered with post-functionalization. Subsequently, we created a composite catalytic system, HCP-PNTL-Co, by introducing cobalt ions (Co^{2+}) through coordination. This system was applied to the cycloaddition of CO_2 with epoxides and the photoreduction of CO_2 under ambient conditions. Among the different types, HCP-PNTL-Co-B, with the highest nitrogen content of 5.6 wt%, demonstrated superior CO_2 adsorption, reaching 2.0 mmol/g at 273 K and 1 bar, and an adsorption heat of 33.0 kJ/mol. This material outperformed HCP-PNTL-Co-A, which had a lower nitrogen content of 2.9 wt%, showing increased catalytic activity and efficiency in both the cycloaddition and photoreduction reactions at ambient conditions. This study illustrates that the direct introduction of CO_2-

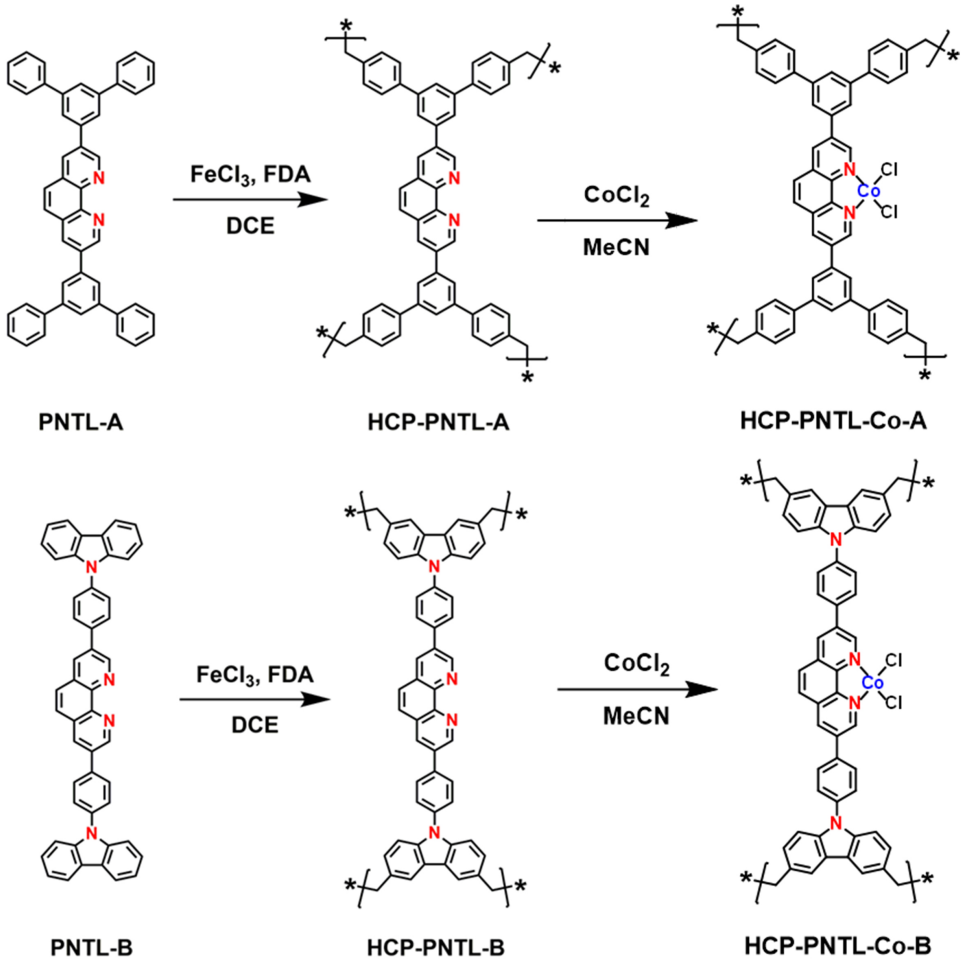

Scheme 1. The synthetic pathway of HCP-PNTL and HCP-PNTL-Co porous network structures. HCP: Hypercrosslinked polymer; PNTL: 1,10-phenanthroline.

philic active sites into HCPs significantly augments both CO_2 adsorption capacity and activation potential, avoiding the need for post-functionalization and ensuring a more uniform distribution of CO_2-philic active sites, thus facilitating the catalytic conversion of CO_2. These findings highlight the potential for efficient CO_2 catalytic conversion, offering a promising approach to addressing the challenges of greenhouse gas emissions and energy scarcity and paving the way for developing and designing new strategies for efficient CO_2 catalytic conversion systems.

EXPERIMENTAL

Materials

Acetonitrile (MeCN), [Gas Chromatography (GC)], 1,3,5-trimethylbenzene (GC), formaldehyde dimethyl acetal, (3,5-diphenylphenyl)boronic acid (98%), 3,8-dibromo-1,10-phenanthroline (98%), (4-(9H-carbazol-9-yl)phenyl)boronic acid (98%), tetrakis (triphenylphosphine) palladium (99%), cobalt chloride hexahydrate [Analytical Reagent (AR)], 4-dimethylaminopyridine (99%), tetraphenylphosphonium bromide (TPPB) (99%), epoxides (AR), triethanolamine (TEOA) (AR), and tris(2,2'-bipyridyl)ruthenium(II) chloride hexahydrate (98%) were purchased from Aladdin Chemical Reagent Corp. Tetrabutylammonium bromide (TBAB) (AR), dichloromethane (AR), 1,2-dichloroethane (AR), HCl (37%), 1,4-dioxane (AR), N,N-dimethylformamide (AR), ethylacetate (AR), tetrahydrofuran (AR), anhydrous potassium carbonate (AR),

magnesium sulfate anhydrous (AR), iron(III) chloride anhydrous [Chemical Reagent (CR)], ethanol (AR), and methanol (AR) were provided from Sinopharm Chemical Reagent Co., Ltd.

Synthesis procedure

Synthesis of porous polymers

The HCP-PNTL-A[54] was synthesized by adding PNTL-A, formaldehyde dimethyl acetal, and 1,2-dichloroethane to a glass flask. Anhydrous $FeCl_3$ was then introduced under a nitrogen atmosphere, followed by stirring at 45 °C for 5 h and 80 °C for 19 h. The resulting solid polymer was collected, washed with methanol and deionized (DI) water, and extracted with methanol using a Soxhlet apparatus. The dried polymer was obtained as a brown solid. The procedure for HCP-PNTL-B[55] was similar, replacing PNTL-A with PNTL-B.

Synthesis of metal-containing polymers

For HCP-PNTL-Co-A synthesis, a mixture of HCP-PNTL-A, cobalt chloride, and MeCN was stirred and refluxed at 65 °C for 12 h under nitrogen. After purification, the product was obtained as a solid. HCP-PNTL-Co-B was synthesized using the same method with HCP-PNTL-B instead of HCP-PNTL-A.

The yields of HCP-PNTL-A, HCP-PNTL-B, HCP-PNTL-Co-A, and HCP-PNTL-Co-B were 132%, 126%, 90%, and 85%, respectively.

RESULTS AND DISCUSSION

Structural and morphological characterizations

Confirmation of successful material synthesis was achieved through Fourier-transform infrared spectroscopy (FT-IR), solid-state ^{13}C cross-polarization/magic angle spinning nuclear magnetic resonance (^{13}C CP/MAS NMR), and elemental analysis (EA). The FT-IR spectra [Figure 1A and B] displayed characteristic absorption peaks at 1,597 and 1,250 cm^{-1}, indicative of the stretching vibrations of C=N and C–N in the pyridine units, respectively. This confirms the stable incorporation of the monomer structure within the polymer framework. Additionally, the presence of characteristic aliphatic C–H stretching vibrations between 2,920-2,860 cm^{-1} signifies the successful execution of the Friedel-Crafts alkylation, indicating the establishment of the hypercrosslinked network. The ^{13}C CP/MAS NMR spectra [Figure 1C] exhibit aromatic carbon peaks at 138 and 131 ppm, verifying the inclusion of aromatic monomers in forming the HCPs. The signal at 39 ppm is attributed to methylene carbons, further evidencing the completion of the Friedel-Crafts alkylation reaction[25], which agrees with the FT-IR results. EA data provided in Supplementary Table 1 reveals that the nitrogen content in HCP-PNTL-B is substantially higher than in HCP-PNTL-A. This is attributed to the higher nitrogen content in the monomers used to synthesize HCP-PNTL-B and aligns with the theoretical expectations. This finding also suggests that the nitrogen content in HCPs can be controlled effectively by varying the nitrogen heteroatom content in the functional monomers used.

The HCPs are demonstrated to possess irregular layered structures by scanning (SEM) and transmission electron microscopy (TEM) images [Supplementary Figure 1]. A uniform distribution of carbon (C), nitrogen (N), and cobalt (Co) within the HCP-PNTL-Co samples is indicated by elemental mapping [Supplementary Figures 2 and 3]. The cobalt content in HCP-PNTL-Co-A and HCP-PNTL-Co-B was determined to be approximately 1.5 wt% and 1.3 wt%, respectively, by inductively coupled plasma optical emission spectrometry (ICP-OES) analysis. Thermogravimetric analysis (TGA) suggests that both HCP-PNTL and HCP-PNTL-Co display thermal stability up to 300 °C in a nitrogen atmosphere [Figure 1D]. The light absorption ability of the polymer was analyzed using ultraviolet (UV)-visible absorption, and Figure 1E

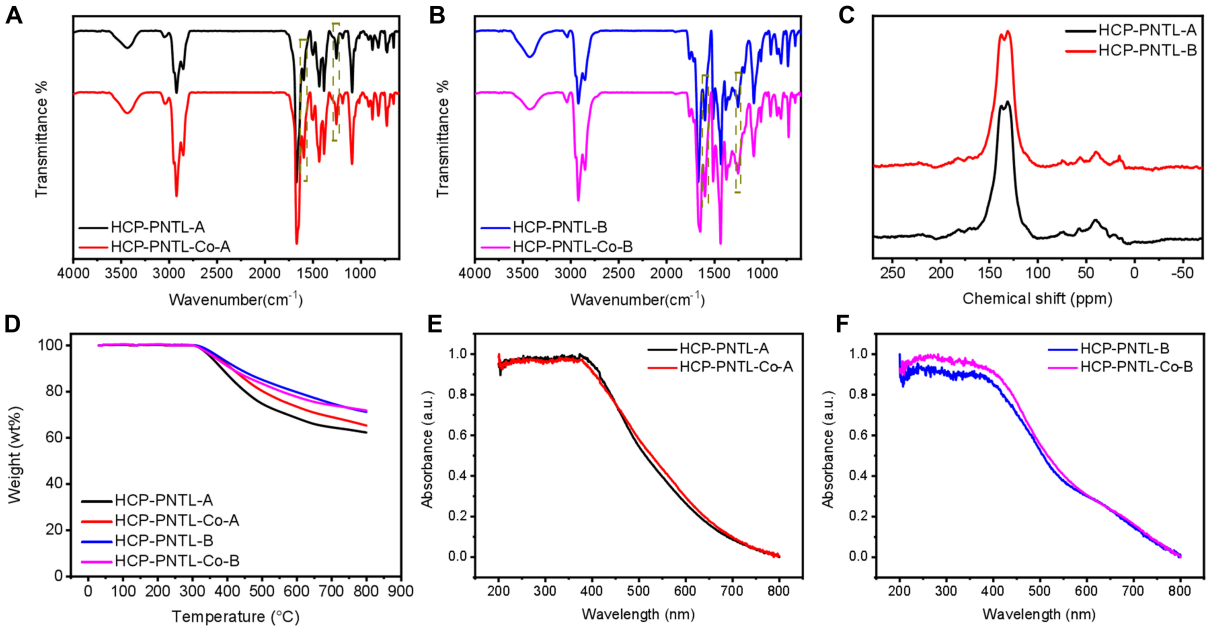

Figure 1. FT-IR spectra (A) and (B), solid-state ^{13}C NMR spectra (C), TGA (D) (measured under N_2 atmosphere), and solid-state UV-visible absorption spectra (E) and (F) of HCP-PNTL and HCP-PNTL-Co. FT-IR: Fourier-transform infrared spectroscopy; NMR: nuclear magnetic resonance; TGA: thermogravimetric analysis; UV: ultraviolet; HCP: hypercrosslinked polymer; PNTL: 1,10-phenanthroline.

and F displays the solid-state UV absorption spectra of HCP-PNTL and HCP-PNTL-Co. All polymers demonstrate strong light absorption in the visible light region, with absorption edges beyond 500 nm. The UV absorption spectrum of HCP-PNTL-Co shows a slight redshift compared to HCP-PNTL, indicating that the introduction of Co^{2+} metal enhances the light absorption ability of the material. X-ray photoelectron spectroscopy (XPS) results included in Figure 2, Supplementary Figures 4 and 5 provide detailed insights into the surface chemical composition and the valence states of the elements present in the HCPs. The high-resolution N1s spectrum for HCP-PNTL-A identifies pyridinic nitrogen (binding energy of 399.3 eV) as the dominant nitrogen species [Figure 2A]. In addition, the appearance of the Co-N characteristic peak [Figure 2B], Co $2p_{1/2}$ (798.2 eV), and Co $2p_{3/2}$ (782.2 eV) [Figure 2C] confirms the successful integration of Co^{2+} into HCP-PNTL-A. For HCP-PNTL-B, both pyridinic and carbazolic nitrogen forms are predominant [Figure 2D]; the appearance of the Co-N characteristic peak [Figure 2E] and Co 2p [Figure 2F] also confirms the successful integration of Co^{2+}.

Porosity characteristics and gas adsorption capacities

The internal porosity of HCP-PNTL and HCP-PNTL-Co was assessed using nitrogen adsorption and desorption isotherms at 77.3 K. Figure 3A shows that the N_2 uptake of HCP-PNTL-A and HCP-PNTL-B sharply increased at low relative pressure ($P/P_0 < 0.001$), indicating their microporous nature. The significant desorption hysteresis at intermediate pressure suggests the presence of mesopores. Upon loading with cobalt metal ions, the nitrogen uptake of HCP-PNTL-Co was notably lower than that of HCP-PNTL [Figure 3A], indicating pore blockage. The Brunauer-Emmett-Teller (BET) surface areas were 951 $m^2 \cdot g^{-1}$ for HCP-PNTL-A and 475 $m^2 \cdot g^{-1}$ for HCP-PNTL-B, while they decreased to 609 $m^2 \cdot g^{-1}$ for HCP-PNTL-Co-A and 147 $m^2 \cdot g^{-1}$ for HCP-PNTL-Co-B [Supplementary Table 2]. Figure 3B depicts the pore size distribution calculated by nonlocal density functional theory (NLDFT), confirming the microporous and mesoporous structures of HCP-PNTL and verifying the blockage of some pores in HCP-PNTL-Co.

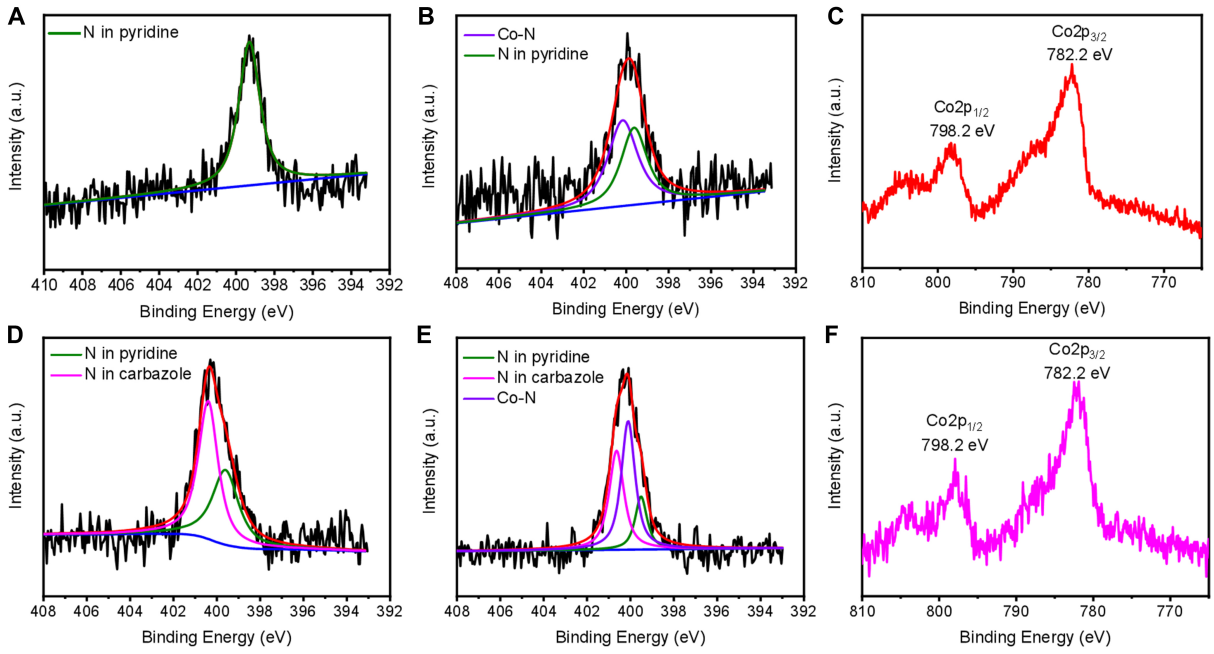

Figure 2. XPS spectra for N1s of (A) HCP-PNTL-A, (B) HCP-PNTL-Co-A, (D) HCP-PNTL-B and (E) HCP-PNTL-Co-B; Co2p of (C) HCP-PNTL-Co-A and (F) HCP-PNTL-Co-B. XPS: X-ray photoelectron spectroscopy; HCP: hypercrosslinked polymer; PNTL: 1,10-phenanthroline.

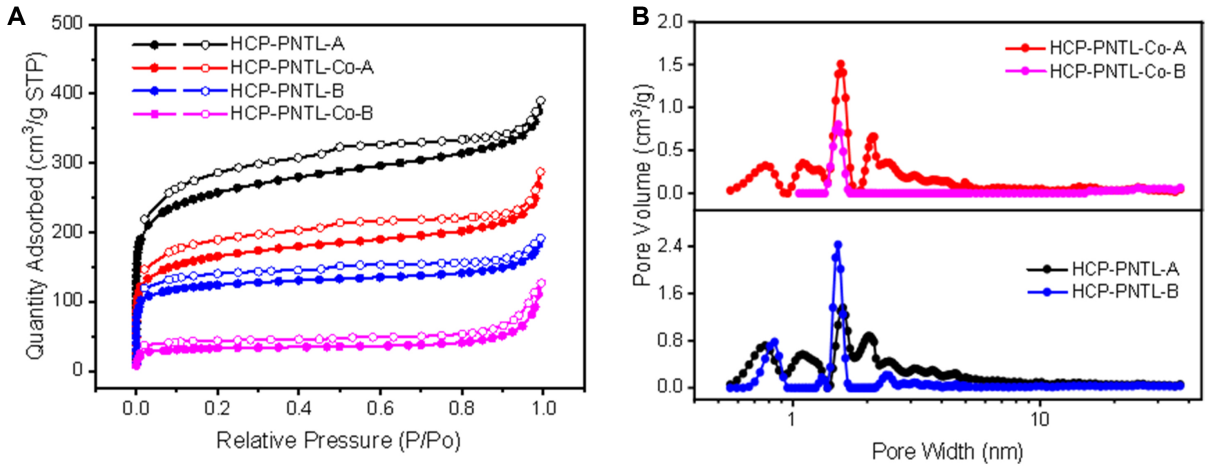

Figure 3. (A) Nitrogen adsorption and desorption isotherms of HCP-PNTL and HCP-PNTL-Co; (B) Pore size distribution calculated using DFT methods of HCP-PNTL and HCP-PNTL-Co. HCP: Hypercrosslinked polymer; PNTL: 1,10-phenanthroline; DFT: density functional theory.

The CO_2 gas adsorption capacity of phenanthroline-based HCPs was assessed based on their high specific surface area, microporosity, and abundant nitrogen atoms [Supplementary Table 2]. Figure 4A and B shows that HCP-PNTL-A has the highest CO_2 adsorption capacity of 3.2 mmol·g^{-1} (1 bar, 273 K) and 1.9 mmol·g^{-1} (1 bar, 298 K), attributed to its highest specific surface area and micropore volume. HCP-PNTL-B with lower specific surface area and micropore volume shows a lower CO_2 uptake (2.2 mmol·g^{-1} at 1 bar/273 K and 1.5 mmol·g^{-1} at 1 bar/298 K) than HCP-PNTL-A. Upon the introduction of metal Co^{2+}, the CO_2 adsorption capacity of HCP-PNTL-Co decreases due to the reduction in specific surface area and micropore volume. The CO_2 uptake of HCP-PNTL-Co-A decreased to 2.2 mmol·g^{-1} at 1 bar/273 K and 1.4 mmol·g^{-1} at

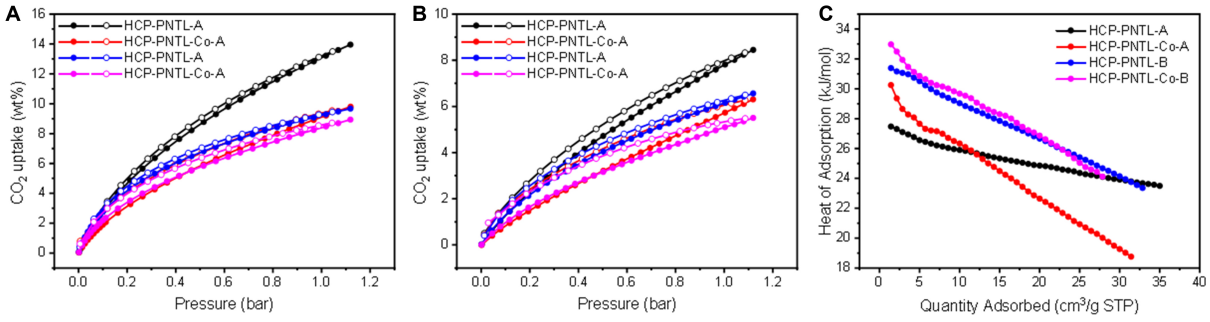

Figure 4. CO_2 adsorption-desorption isotherms at (A) 273.15 K and (B) 298.15 K of HCP-PNTL and HCP-PNTL-Co; isosteric heat of adsorption (C) of HCP-PNTL and HCP-PNTL-Co. HCP: Hypercrosslinked polymer; PNTL: 1,10-phenanthroline.

1 bar/298 K [Figure 4A and B]. HCP-PNTL-Co-B still shows high CO_2 adsorption capacity (2.0 mmol·g^{-1} at 1 bar/273 K and 1.3 mmol·g^{-1} at 1 bar/298 K) even though the BET specific surface area is only 147 m^2·g^{-1}, which is due to the interaction between the material and CO_2 enhanced by abundant N atoms and Co^{2+} in the structure. The above results indicate that the prepared HCPs rich in N atoms possess good CO_2 adsorption performance, which is conducive to increasing the CO_2 concentration near the catalytic sites and further promoting the CO_2 catalytic conversion under the ambient conditions. In addition, there is little difference in the CO_2 adsorption capacity between HCP-PNTL-Co-A and HCP-PNTL-Co-B, which is beneficial for comparing the subsequent CO_2 catalytic activity and identifying the factors affecting the activity. The isosteric heats of adsorption (Qst) was calculated from CO_2 adsorption isotherms at different temperatures (273 and 298 K) using the Clausius-Clapeyron equation to understand the adsorption properties between phenanthroline-based HCPs and CO_2 molecules [Figure 4C]. The onset Qst value of HCP-PNTL-B (31.4 kJ·mol^{-1}) was notably higher than that of HCP-PNTL-A (27.5 kJ·mol^{-1}), suggesting a stronger interaction between CO_2 and HCP-PNTL-B, which has a higher nitrogen content. This stronger interaction is beneficial for activating CO_2 to promote subsequent conversion reactions. Additionally, the Qst value increased with the introduction of metal Co^{2+}. The onset Qst values for HCP-PNTL-Co-A and HCP-PNTL-Co-B were 30.3 and 33.0 kJ·mol^{-1}, respectively. This result also indicates that HCP-PNTL-Co-B has stronger adsorption force on CO_2 and can activate inert CO_2 molecules effectively, thus improving the catalytic efficiency of CO_2.

Catalytic performance of cycloaddition

The application of HCP-PNTL-Co in the CO_2 cycloaddition reaction with epoxides was initially explored using propylene oxide (PO) as the substrate. As shown in Table 1, the reaction failed to occur in the absence of catalyst and cocatalyst (entry 1). Nevertheless, the conversion yields of PO were limited without the inclusion of catalyst (21%, Table 1, entry 2) or cocatalyst (7% or 9%, Table 1, entry 3 or entry 4), indicating that both catalyst and cocatalyst are indispensable in the cycloaddition reaction. The conversion yield of PO with HCP-PNTL-Co-A reached 75% in the presence of TBAB at 48 h, realizing a relatively efficient CO_2 conversion under ambient conditions (Table 1, entry 5). In contrast, HCP-PNTL-Co-B displayed higher activity than HCP-PNTL-Co-A; a high yield of up to 95% was obtained in 48 h with the turnover number (TON) [turnover frequency (TOF)] of 5,380 (112 h^{-1}). By comparing the activity of other catalysts in the table [Supplementary Table 3], it can be seen that HCP-PNTL-Co-B is also superior to most reported heterogeneous catalysts under mild conditions. It has significant advantages in TON (5,380) compared to some catalysts with high TON values, such as 2,2'-bipyridine zinc(II)-based hierarchical meso/microporous polymers (Bp-Zn@MA) (3,378)[56]; COF-salen-Co (3,744)[57]; P-POF-Zn (33,323)[58], *etc.* Although the specific surface area of HCP-PNTL-Co-B is smaller than that of HCP-PNTL-Co-A, HCP-PNTL-Co-B has a higher nitrogen content. Considering the small difference in the adsorption capacity of CO_2 and Co^{2+}

Table 1. Catalytic coupling of CO_2 and PO using various catalytic systems[a]

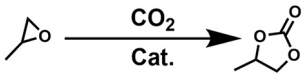

Entry	Catalyst	TBAB	Substrate	Time (h)	Yield[b] (%)	TON (TOF·h^{-1})
1	None	None	PO	48	0	-
2	None	1.2 mmol	PO	48	21	-
3	HCP-PNTL-Co-A	None	PO	48	7	344 (7)
4	HCP-PNTL-Co-B	None	PO	48	9	663 (14)
5	HCP-PNTL-Co-A	1.2 mmol	PO	48	75	3,681 (77)
6	HCP-PNTL-Co-B	1.2 mmol	PO	48	95	5,380 (112)

[a]Cycloaddition reaction conditions: 25 mmol substrate (PO) with 20 mg catalyst, CO_2 (0.1 MPa), 25 °C. [b]Isolated yields judged by GC. PO: Propylene oxide; TBAB: tetrabutylammonium bromide; TON: turnover number; TOF: turnover frequency; HCP: hypercrosslinked polymer; PNTL: 1,10-phenanthroline; GC: gas chromatography.

content between HCP-PNTL-Co-A and HCP-PNTL-Co-B, the higher catalytic performance of HCP-PNTL-Co-B may be due to the stronger adsorption of CO_2 by HCP-PNTL-Co-B with higher nitrogen content, which concentrates CO_2 around the catalytic sites[46-49]. This process not only increases the concentration of CO_2 but also activates the inert CO_2 molecules adsorbed on the surface, thereby improving the conversion efficiency[59]. It can more effectively activate the adsorbed CO_2 molecules to excited states, making them easier to convert. At the same time, the above results also reveal that the effective activation of CO_2 molecules is crucial for improving the efficiency of CO_2 catalytic conversion. The possible mechanism of the HCP-PNTL-Co catalyzed CO_2 cycloaddition is shown in Supplementary Figure 6.

Further investigations were conducted on the effects of reaction conditions, including reaction time, various cocatalysts, and the amount of cocatalyst TBAB, using HCP-PNTL-Co-B under mild conditions (0.1 MPa, 25 °C). The yield of propylene carbonate (PC) was only 39% within the first 12 h of reaction, despite the rapid conversion of PO during this period [Figure 5A]. Moreover, the yield of product gradually increased by further prolonging the reaction time, and the PC yield could reach 95% within 48 h. Subsequently, the effects of different cocatalysts on the PO conversion were investigated under the same conditions (0.1 MPa, 25 °C). Figure 5B showed that the conversion of PO was only 46% with N,N-Dimethylpyridin-4-amine (DMAP) as the cocatalyst, while the PC yield increased dramatically to 95% or 89% when TBAB or TPPB was employed as the cocatalyst. Since the highest yield was achieved when TBAB was used as a cocatalyst, it was selected as the optimal cocatalyst for the catalytic reaction. The effects of cocatalyst (TBAB) amount on the cycloaddition reactions were also evaluated using HCP-PNTL-Co-B [Figure 5C]. The yield of PC could still reach 75% when the amount of TBAB was only 0.6 mmol, illustrating the high catalytic activity of HCP-PNTL-Co-B for cycloaddition reactions. As the amount of TBAB increased, the PC yield also increased from 75% to 95%. The preceding results indicated the optimal reaction conditions for the catalytic system as follows: a reaction duration of 48 h, employing TBAB as a cocatalyst at a quantity of 1.2 mmol.

Reusability is a key factor in heterogeneous catalysis; the reusability and structural stability of HCP-PNTL-Co-B were evaluated. As shown in Figure 5D, HCP-PNTL-Co-B maintained the high efficiency after six cycles, which showed good cycling stability. The structural characterization of spent HCP-PNTL-Co-B revealed identical FT-IR spectra [Supplementary Figure 7] to that of fresh HCP-PNTL-Co-B, which confirms their excellent recycling catalytic behavior. Diversifying the range of substrates with HCP-PNTL-Co-B as the catalyst, the catalytic system demonstrated effectiveness with various terminal epoxides as well [Table 2]. Various epoxides were effectively transformed into their respective cyclic carbonates, yielding

Table 2. Different substituted epoxides were catalytically coupled with CO_2 using HCP-PNTL-Co-B under ambient conditions of room temperature and atmospheric pressure[a]

Entry	Epoxides	Products	Time (h)	Yields[b] (%)	TON
1		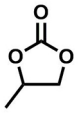	48	95	5,380
2		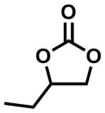	48	94	5,323
3		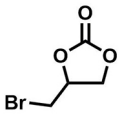	48	95	5,380
4		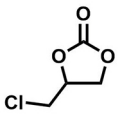	48	95	5,380
5		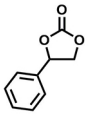	48	89	5,040
6	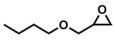	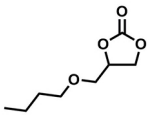	48	94	5,323
7	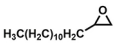	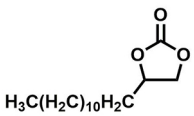	48	92	5,213

[a]Cycloaddition reaction conditions: 25 mmol substrate with 20 mg catalyst, CO_2 (0.1 MPa), 25 °C. [b]Isolated yields determined by GC. HCP: Hypercrosslinked polymer; PNTL: 1,10-phenanthroline; TON: turnover number; GC: gas chromatography.

high percentages of 89%-95% and high TONs of 5,040-5,380. The more inert 2, 3-epoxide propyl butyl ether (entry 6) and 1, 2-epoxide tetradecane (entry 7) can also be efficiently converted with yields of 94% and 92%, respectively. These results show that HCP-PNTL-Co-B has good universality and can catalyze different types of epoxy substrates efficiently. The products of the CO_2 conversion reaction were identified by ^1H NMR spectra [Supplementary Figures 8-14].

Photocatalytic performances for CO_2 reduction

To investigate the photoelectric characteristics and applicability of HCP-PNTL and HCP-PNTL-Co for photocatalytic reduction of CO_2, solid-state UV-vis spectroscopy measurement was performed. As illustrated in Figure 1E and F, all polymers exhibited a wide and strong visible-light absorption region up to approximately 500 nm, while the absorption edge of HCP-PNTL-Co had a slight redshift, indicating a slight enhancement of light absorption capability with the introduction of metal Co^{2+}. The results of the UV-vis spectroscopy indicate that HCP-PNTL-Co has strong light absorption capacity, providing a guarantee for the photocatalytic CO_2 reduction under visible light.

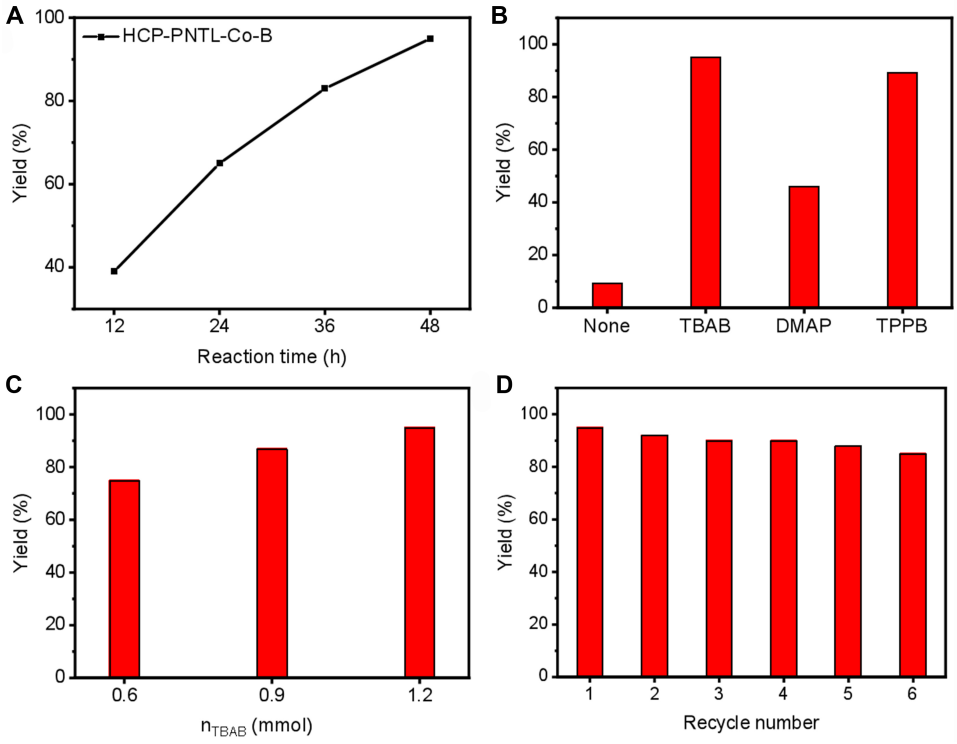

Figure 5. Influence of (A) reaction time, (B) different cocatalysts and (C) amount of TBAB on the catalytic performance of HCP-PNTL-Co-B; (D) Recyclability of HCP-PNTL-Co-B for the chemical conversion of CO_2 under ambient conditions of room temperature and atmospheric pressure. TBAB: tetrabutylammonium bromide; HCP: hypercrosslinked polymer; PNTL: 1,10-phenanthroline.

The photocatalytic performance of HCP-PNTL-Co was studied using $[Ru(bpy)_3]Cl_2$ as the photosensitizer and TEOA as the sacrificial agent in a mixed solvent of MeCN and H_2O under 1 atm CO_2 and visible light irradiation. Figure 6A illustrates the time-dependent yields of CO and H_2 for HCP-PNTL-Co. HCP-PNTL-Co-B demonstrated the highest photocatalytic activity, with production rates of CO and H_2 reaching 2,173 and 414 $\mu mol \cdot g^{-1} \cdot h^{-1}$ after three hours, respectively, resulting in a CO selectivity of 84%.The photocatalytic activity of HCP-PNTL-Co-A was slightly inferior to that of HCP-PNTL-Co-B, exhibiting lower production rates of CO and H_2 of 1,726 and 491 $\mu mol \cdot g^{-1} \cdot h^{-1}$, respectively, and a CO selectivity of 78%. Given the slight variance in CO_2 adsorption capability between HCP-PNTL-Co-A and HCP-PNTL-Co-B, the higher catalytic efficiency may be attributed to the stronger adsorption force between HCP-PNTL-Co-B with higher N contents and CO_2, which can activate the adsorbed CO_2 molecules to excited states more effectively, thereby facilitating their conversion. The results of CO_2 photocatalytic reduction were consistent with the above cycloaddition reactions, indicating that HCP-PNTL-Co-A and HCP-PNTL-Co-B with abundant N heteroatoms have high CO_2 photocatalytic reduction ability. Furthermore, this clearly demonstrates the potential of metal ion doping in HCPs for photocatalytic CO_2 reduction and the effectiveness of introducing CO_2-philic active sites to enhance CO_2 catalytic conversion efficiency. The photocatalytic performance of HCP-PNTL-B modified with other metal ions such as Fe^{2+}, Mn^{2+}, or Ni^{2+} was evaluated under identical reaction conditions, and the chemical structure, thermal stability and porosity characteristics and gas adsorption capacities were performed [Supplementary Figures 15-20]. As shown in Figure 6B, HCP-PNTL-Ni-B exhibits the highest catalytic activity, producing a large amount of CO (2,761 $\mu mol \cdot g^{-1} \cdot h^{-1}$) and a small amount of H_2 (307 $\mu mol \cdot g^{-1} \cdot h^{-1}$), with a high selectivity for CO production (90%). The highest catalytic activity and selectivity of HCP-PNTL-Ni-B can be attributed to the minimal energy barrier of nickel metal in the reaction process[60]. The catalytic performance of HCP-PNTL-Ni-B is

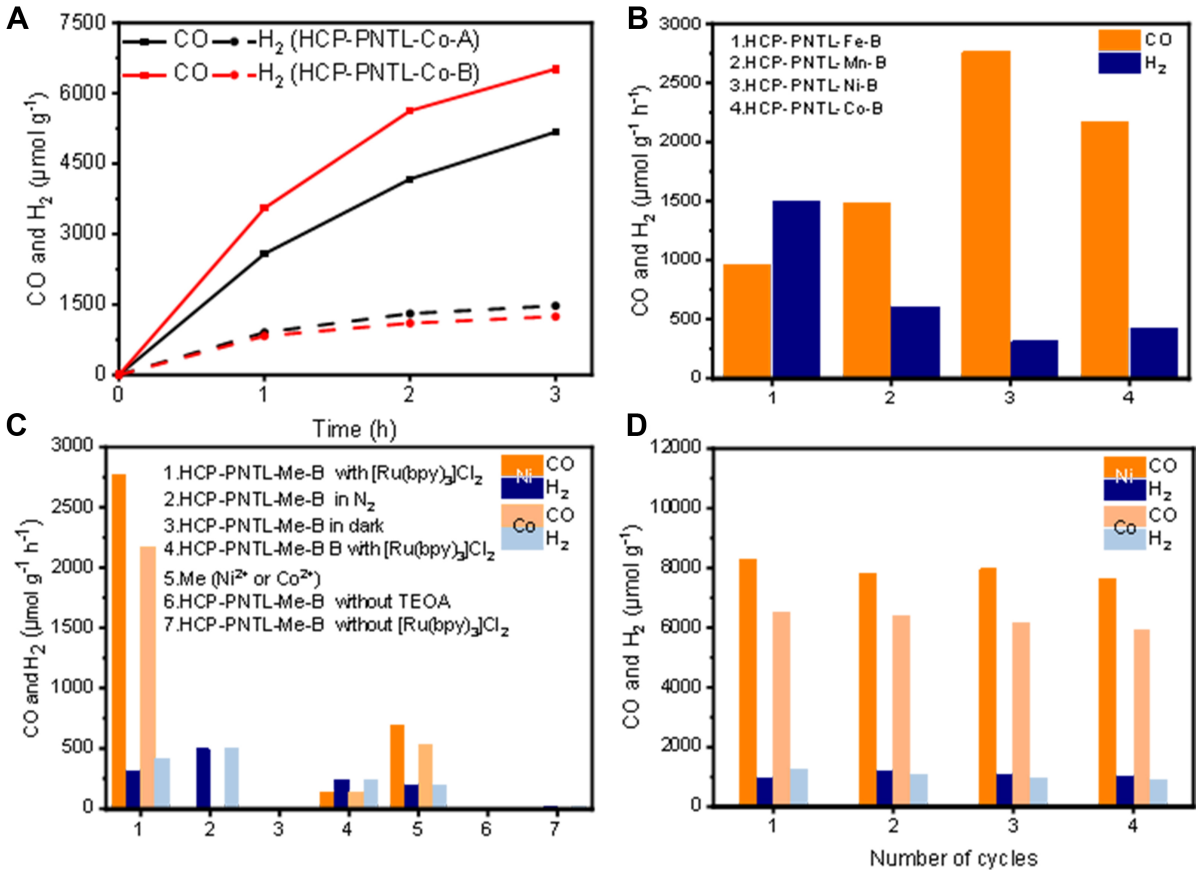

Figure 6. The production rate of CO and H_2 evolution over (A) HCP-PNTL-Co and (B) HCP-PNTL-M-B under visible-light irradiation; (C) The production rate of CO and H_2 evolution under various conditions of HCP-PNTL-Ni-B and HCP-PNTL-Co-B; (D) Cyclic stability test of HCP-PNTL-Ni-B and HCP-PNTL-Co-B. HCP: Hypercrosslinked polymer; PNTL: 1,10-phenanthroline.

comparable to that of the majority of previously reported metal-modified COFs/covalent triazine frameworks (CTFs)-based photocatalytic systems operating under similar reaction conditions [Supplementary Table 4]. The CO production rate of HCP-PNTL-Ni-B is 2,761 μmol·g^{-1}·h^{-1}, significantly higher than most other systems, such as Co@COF-TVBT-Bpy (1,133 μmol·g^{-1}·h^{-1})[61], 3,3',5,5'-Tetraformyl-4,4'-biphenyldiol (TFBD)-COF-Co-salicylideneaniline (SA) (1,480 μmol·g^{-1}·h^{-1})[62], *etc.* The CO selectivity of HCP-PNTL-Ni-B is 90%, which is comparable to other systems, such as TFBD-COF-Co-SA (90%)[62], Ni-TpBpy[constructed from triformylphloroglucinol (Tp) and 2,2'-bipyridine (Bpy)]-COF (96%)[63], and Ni-COFs (95%)[64].

Control experiments were conducted to ascertain the influence of various reaction factors in the photocatalytic system [Figure 6C]. The production rate of CO was only 136 μmol·g^{-1}·h^{-1} with HCP-PNTL-B as the catalyst for photocatalytic CO_2 reduction, and the selectivity for CO was only 36.8%, indicating that metal Ni^{2+} or Co^{2+} is the catalytic active site for photocatalytic CO_2 reduction. Under the condition of using metal Ni^{2+} or Co^{2+} alone as the catalyst, the production rate and selectivity of CO was only 683 μmol·g^{-1}·h^{-1} and 78% or 533 μmol·g^{-1}·h^{-1} and 73%, much lower than that of HCP-PNTL-Ni-B or HCP-PNTL-Co-B, indicating that the existence of HCP-PNTL-B in the catalytic system improved the CO_2 adsorption and activation ability and the stable dispersion of Ni^{2+} or Co^{2+} catalytic sites, which can significantly enhance the photocatalytic CO_2 reduction performance. When the photosensitizer was absent from the reaction system,

only trace amounts of CO and H_2 were detectable, while negligible amounts were obtained without a sacrificial agent or light irradiation during the photocatalytic reduction reaction. Substituting N_2 for CO_2 in the photocatalytic reaction resulted in a significant amount of H_2 (492 μmol·g^{-1}·h^{-1}) but no detectable CO. The control experiments demonstrated the essential nature of all the previously mentioned reaction factors for the photocatalytic conversion of CO_2. Lastly, the impact of solvents on the photocatalytic CO_2 reduction performance of HCP-PNTL-Ni-B was examined. As shown in Supplementary Figure 21, HCP-PNTL-Ni-B exhibited the optimal photocatalytic activity in MeCN. The higher photocatalytic performance may be that, compared to other solvents, MeCN has a higher solubility for CO_2, which is conducive to the increase of CO_2 concentration near the catalytic sites. Similar reaction mechanisms for the catalytic reduction of CO_2 by metal-based POPs photocatalytic systems under catalytic conditions have been reported in related studies. Based on literature reports[64,65] and control experimental results, the possible mechanism of HCP-PNTL-Ni-B catalyzing CO_2 reduction was speculated based on the action of non-conjugated metal adjacent phenanthroline-based HCPs in providing metal catalytic sites and enhancing the CO_2 concentration near the catalytic sites. First, the photosensitizer $[Ru(bpy)_3]Cl_2$ generates electron-hole pairs under visible light excitation. Subsequently, the excited state $Ru(bpy)_3^{2+}$ is quenched back to the ground state by the sacrificial agent TEOA, and some electrons are transferred to HCP-PNTL-Ni-B, where the adsorbed CO_2 accepts electrons and is reduced to CO.

To confirm the source of CO, isotope-labeled $^{13}CO_2$ was utilized as the substrate for the photocatalytic reaction under identical conditions, and the resulting product was identified using gas chromatography-mass spectrometry (GC-MS). As shown in Supplementary Figure 22, the presence of a peak at m/z = 29 indicated that the generated ^{13}CO originated from gaseous $^{13}CO_2$ species rather than the decomposition of other organic compounds, such as the photocatalyst or solvent, in the photocatalytic system. It can be seen from Figure 6D that there was no obvious loss of the photocatalytic activity of HCP-PNTL-Ni-B or HCP-PNTL-Co-B after four-run cycling experiments, verifying its superior reusability in the photocatalytic reaction. Furthermore, negligible changes were observed in the FT-IR spectra [Supplementary Figure 23] of HCP-PNTL-Ni-B before and after the photocatalytic cycling reactions, confirming the structural stability and photocatalytic durability of HCP-PNTL-Ni-B in the photocatalytic CO_2 reduction process.

CONCLUSIONS

In summary, PNTL derivatives were selected as functional monomers for the HCP synthesis via the Friedel-Crafts reaction. Subsequently, a composite catalytic system was devised by incorporating Co^{2+} for use in the cycloaddition reaction of CO_2 with epoxides and the photoreduction of CO_2 under ambient conditions. The nitrogen content in the structure of HCPs was enhanced by directly regulating the structure of the functional monomer to increase the CO_2 adsorption capacity and activation ability, which can avoid the uneven distribution of CO_2-philic active sites introduced by post-functionalization. The composite catalytic system with the highest nitrogen content (5.6 wt%), HCP-PNTL-Co-B, achieved CO_2 adsorption capacity and heat of adsorption of 2.0 mmol/g (273 K, 1 bar) and 33.0 kJ·mol^{-1}, respectively. In the presence of cocatalyst TBAB, HCP-PNTL-Co-B also showed higher catalytic activity, achieving efficient catalysis of the cycloaddition reaction of CO_2 with epoxides under ambient pressure and temperature with a high yield of 95% after 48 h and a TON (TOF) value of up to 5,380 (112 h^{-1}). Meanwhile, HCP-PNTL-Co-B also achieved a high CO production rate of 2,173 μmol·g^{-1}·h^{-1} and a high selectivity of 84% in the photoreduction reaction. Moreover, the composite catalytic system exhibited good structural stability in the cycling experiments. The study has shown that introducing CO_2-philic active sites improves the CO_2 adsorption and activation capacity of materials, offering a novel research strategy for developing and designing efficient CO_2 catalytic systems. Future research efforts can be conducted in-depth and systematically around (1) enhancing the conversion efficiency of materials for CO_2 under mild conditions by adjusting the microstructure of

catalysts or optimizing reaction conditions; (2) improving the structural stability of materials to ensure their efficient performance during cycling; (3) elucidating the catalytic mechanism and establishing the structure-performance relationship between polymer structure and catalytic properties.

DECLARATIONS

Acknowledgments

The authors thank the Analysis and Testing Center at Huazhong University of Science and Technology for their assistance in the characterization of materials.

Authors' contributions

Made substantial contributions to conception and design of the study and performed data analysis and interpretation: Ouyang H, Peng M

Performed data acquisition and provided administrative, technical, and material support: Song K, Wang S, Gao H, Tan B

Availability of data and materials

The authors confirm that the data supporting the findings of this study are available within its Supplementary Materials.

Financial support and sponsorship

This work was financially supported by the National Natural Science Foundation of China (Grant Nos. 22161142005, 21975086), the International S&T Cooperation Program of China (Grant No. 2018YFE0117300), Science and Technology Department of Hubei Province (No. 2019CFA008), and the Open Research Fund (No. 2023JYBKF04) of Key Laboratory of Material Chemistry for Energy Conversion and Storage (HUST), Ministry of Education.

Conflicts of interest

All authors declared that there are no conflicts of interest.

Ethical approval and consent to participate

Not applicable.

Consent for publication

Not applicable.

Copyright

© The Author(s) 2024.

REFERENCES

1. Ji, G.; Zhao, Y.; Liu, Z. Design of porous organic polymer catalysts for transformation of carbon dioxide. *Green. Chem. Eng.* **2022**, *3*, 96-110. DOI
2. Truong, C. C.; Mishra, D. K. Catalyst-free fixation of carbon dioxide into value-added chemicals: a review. *Environ. Chem. Lett.* **2021**, *19*, 911-40. DOI
3. Cheng, Y.; Ding, X.; Han, B. Porous organic polymers for photocatalytic carbon dioxide reduction. *ChemPhotoChem* **2021**, *5*, 406-17. DOI
4. Zhang, X. Y.; Wang, P.; Zhang, Y.; Cheng, X. M.; Sun, W. Y. Facet-dependent photocatalytic behavior of Fe-soc-MOF for carbon dioxide reduction. *ACS. Appl. Mater. Interfaces.* **2023**, *15*, 3348-56. DOI PubMed
5. Steinlechner, C.; Junge, H. Renewable methane generation from carbon dioxide and sunlight. *Angew. Chem. Int. Ed. Engl.* **2018**, *57*, 44-5. DOI PubMed
6. Liao, X.; Wang, Z.; Kong, L.; et al. Synergistic catalysis of hypercrosslinked ionic polymers with multi-ionic sites for conversion of

CO_2 to cyclic carbonates. *Mol. Catal.* **2023**, *535*, 112834. DOI
7. Li, P. Z.; Wang, X. J.; Liu, J.; Lim, J. S.; Zou, R.; Zhao, Y. A triazole-containing metal-organic framework as a highly effective and substrate size-dependent catalyst for CO_2 conversion. *J. Am. Chem. Soc.* **2016**, *138*, 2142-5. DOI PubMed
8. Truong, C. C.; Mishra, D. K. Recent advances in the catalytic fixation of carbon dioxide to value-added chemicals over alkali metal salts. *J. CO2. Util.* **2020**, *41*, 101252. DOI
9. Zhao, Y.; Han, B.; Liu, Z. Ionic-liquid-catalyzed approaches under metal-free conditions. *Acc. Chem. Res.* **2021**, *54*, 3172-90. DOI PubMed
10. Chen, Y.; Mu, T. Conversion of CO_2 to value-added products mediated by ionic liquids. *Green. Chem.* **2019**, *21*, 2544-74. DOI
11. Aomchad, V.; Del, G. S.; Yingcharoen, P.; Poater, A.; D'elia, V. Exploring the potential of group III salen complexes for the conversion of CO_2 under ambient conditions. *Catal. Today.* **2021**, *375*, 324-34. DOI
12. Lan, D.; Gong, Y.; Tan, N.; et al. Multi-functionalization of GO with multi-cationic ILs as high efficient metal-free catalyst for CO_2 cycloaddition under mild conditions. *Carbon* **2018**, *127*, 245-54. DOI
13. Cui, X.; Dai, X.; Surkus, A.; et al. Zinc single atoms on N-doped carbon: an efficient and stable catalyst for CO_2 fixation and conversion. *Chinese. J. Catal.* **2019**, *40*, 1679-85. DOI
14. Jayakumar, S.; Li, H.; Tao, L.; et al. Cationic Zn-porphyrin immobilized in mesoporous silicas as bifunctional catalyst for CO_2 cycloaddition reaction under cocatalyst free conditions. *ACS. Sustain. Chem. Eng.* **2018**, *6*, 9237-45. DOI
15. Miralda, C. M.; Macias, E. E.; Zhu, M.; Ratnasamy, P.; Carreon, M. A. Zeolitic imidazole framework-8 catalysts in the conversion of CO_2 to chloropropene carbonate. *ACS. Catal.* **2012**, *2*, 180-3. DOI
16. Zhu, M.; Srinivas, D.; Bhogeswararao, S.; Ratnasamy, P.; Carreon, M. A. Catalytic activity of ZIF-8 in the synthesis of styrene carbonate from CO_2 and styrene oxide. *Catal. Commun.* **2013**, *32*, 36-40. DOI
17. Ding, M.; Jiang, H. Incorporation of imidazolium-based poly(ionic liquid)s into a metal-organic framework for CO_2 capture and conversion. *ACS. Catal.* **2018**, *8*, 3194-201. DOI
18. Sun, Q.; Aguila, B.; Perman, J.; Nguyen, N.; Ma, S. Flexibility matters: cooperative active sites in covalent organic framework and threaded ionic polymer. *J. Am. Chem. Soc.* **2016**, *138*, 15790-6. DOI PubMed
19. Zhi, Y.; Shao, P.; Feng, X.; et al. Covalent organic frameworks: efficient, metal-free, heterogeneous organocatalysts for chemical fixation of CO_2 under mild conditions. *J. Mater. Chem. A.* **2018**, *6*, 374-82. DOI
20. Sun, Q.; Dai, Z.; Meng, X.; Xiao, F. S. Porous polymer catalysts with hierarchical structures. *Chem. Soc. Rev.* **2015**, *44*, 6018-34. DOI PubMed
21. Zhang, Y.; Riduan, S. N. Functional porous organic polymers for heterogeneous catalysis. *Chem. Soc. Rev.* **2012**, *41*, 2083-94. DOI PubMed
22. Ma, D.; Li, J.; Liu, K.; Li, B.; Li, C.; Shi, Z. Di-ionic multifunctional porous organic frameworks for efficient CO_2 fixation under mild and co-catalyst free conditions. *Green. Chem.* **2018**, *20*, 5285-91. DOI
23. Liu, J.; Zhao, G.; Cheung, O.; Jia, L.; Sun, Z.; Zhang, S. Highly porous metalloporphyrin covalent ionic frameworks with well-defined cooperative functional groups as excellent catalysts for CO_2 cycloaddition. *Chemistry* **2019**, *25*, 9052-9. DOI PubMed
24. Bhanja, P.; Modak, A.; Bhaumik, A. Porous organic polymers for CO_2 storage and conversion reactions. *ChemCatChem* **2019**, *11*, 244-57. DOI
25. Li, B.; Gong, R.; Wang, W.; et al. A new strategy to microporous polymers: knitting rigid aromatic building blocks by external cross-linker. *Macromolecules* **2011**, *44*, 2410-4. DOI
26. Gu, Y.; Son, S. U.; Li, T.; Tan, B. Low-cost hypercrosslinked polymers by direct knitting strategy for catalytic applications. *Adv. Funct. Mater.* **2021**, *31*, 2008265. DOI
27. Tan, L.; Tan, B. Functionalized hierarchical porous polymeric monoliths as versatile platforms to support uniform and ultrafine metal nanoparticles for heterogeneous catalysis. *Chem. Eng. J.* **2020**, *390*, 124485. DOI
28. Gao, T. N.; Wang, T.; Wu, W.; et al. Solvent-induced self-assembly strategy to synthesize well-defined hierarchically porous polymers. *Adv. Mater.* **2019**, *31*, 1806254. DOI PubMed
29. Wang, S.; Zhang, C.; Shu, Y.; et al. Layered microporous polymers by solvent knitting method. *Sci. Adv.* **2017**, *3*, e1602610. DOI PubMed PMC
30. Li, J.; Han, Y.; Ji, T.; et al. Porous metallosalen hypercrosslinked ionic polymers for cooperative CO_2 cycloaddition conversion. *Ind. Eng. Chem. Res.* **2020**, *59*, 676-84. DOI
31. Liao, X.; Wang, Z.; Li, Z.; et al. Tailoring hypercrosslinked ionic polymers with high ionic density for rapid conversion of CO_2 into cyclic carbonates at low pressure. *Chem. Eng. J.* **2023**, *471*, 144455. DOI
32. Wang, S.; Song, K.; Zhang, C.; Shu, Y.; Li, T.; Tan, B. A novel metalporphyrin-based microporous organic polymer with high CO_2 uptake and efficient chemical conversion of CO_2 under ambient conditions. *J. Mater. Chem. A.* **2017**, *5*, 1509-15. DOI
33. Xu, W.; Chen, M.; Yang, Y.; et al. Construction of aluminum-porphyrin-based hypercrosslinked ionic polymers (HIPs) by direct knitting approach for CO_2 capture and in-situ conversion to cyclic carbonates. *ChemCatChem* **2023**, *15*, e202201441. DOI
34. Kunitski, M.; Eicke, N.; Huber, P.; et al. Double-slit photoelectron interference in strong-field ionization of the neon dimer. *Nat. Commun.* **2019**, *10*, 1. DOI PubMed PMC
35. Zhan, Z.; Wang, H.; Huang, Q.; et al. Grafting hypercrosslinked polymers on TiO_2 surface for anchoring ultrafine Pd nanoparticles: dramatically enhanced efficiency and selectivity toward photocatalytic reduction of CO_2 to CH_4. *Small* **2022**, *18*, e2105083. DOI PubMed

36. Manigrasso, J.; Chillón, I.; Genna, V.; et al. Author correction: visualizing group II intron dynamics between the first and second steps of splicing. *Nat. Commun.* **2022**, *13*, 1. DOI PubMed PMC
37. Chen, Y.; Luo, R.; Xu, Q.; Zhang, W.; Zhou, X.; Ji, H. State-of-the-art aluminum porphyrin-based heterogeneous catalysts for the chemical fixation of CO_2 into cyclic carbonates at ambient conditions. *ChemCatChem* **2017**, *9*, 767-73. DOI
38. Yuan, Y. C.; Mellah, M.; Schulz, E.; David, O. R. P. Making chiral salen complexes work with organocatalysts. *Chem. Rev.* **2022**, *122*, 8841-83. DOI PubMed
39. Liao, X.; Xiang, X.; Wang, Z.; et al. A novel crosslinker for synthesizing hypercrosslinked ionic polymers containing activating groups as efficient catalysts for the CO_2 cycloaddition reaction. *Sustain. Energy. Fuels.* **2022**, *6*, 2846-57. DOI
40. Li, H. B.; Yu, M. H.; Wang, F. X.; et al. Amorphous nickel hydroxide nanospheres with ultrahigh capacitance and energy density as electrochemical pseudocapacitor materials. *Nat. Commun.* **2013**, *4*, 1894. DOI PubMed PMC
41. Li, P.; Wang, X.; Liu, J.; Phang, H. S.; Li, Y.; Zhao, Y. Highly effective carbon fixation via catalytic conversion of CO_2 by an acylamide-containing metal-organic framework. *Chem. Mater.* **2017**, *29*, 9256-61. DOI
42. Dai, Z.; Sun, Q.; Liu, X.; et al. Metalated porous porphyrin polymers as efficient heterogeneous catalysts for cycloaddition of epoxides with CO_2 under ambient conditions. *J. Catal.* **2016**, *338*, 202-9. DOI
43. Li, J.; Han, Y.; Lin, H.; et al. Cobalt-salen-based porous ionic polymer: the role of valence on cooperative conversion of CO_2 to cyclic carbonate. *ACS. Appl. Mater. Interfaces.* **2020**, *12*, 609-18. DOI PubMed
44. Xie, Y.; Liang, J.; Fu, Y.; et al. Hypercrosslinked mesoporous poly(ionic liquid)s with high ionic density for efficient CO_2 capture and conversion into cyclic carbonates. *J. Mater. Chem. A.* **2018**, *6*, 6660-6. DOI
45. Ma, Y.; Tang, Q.; Sun, W.; et al. Assembling ultrafine TiO_2 nanoparticles on UiO-66 octahedrons to promote selective photocatalytic conversion of CO_2 to CH_4 at a low concentration. *Appl. Catal. B. Environ.* **2020**, *270*, 118856. DOI
46. Liu, M.; Shao, L.; Huang, J.; Liu, Y. O-containing hyper-cross-linked polymers and porous carbons for CO_2 capture. *Micropor. Mesopor. Mater.* **2018**, *264*, 104-11. DOI
47. Liao, C.; Liang, Z.; Liu, B.; Chen, H.; Wang, X.; Li, H. Phenylamino-, phenoxy-, and benzenesulfenyl-linked covalent triazine frameworks for CO_2 capture. *ACS. Appl. Nano. Mater.* **2020**, *3*, 2889-98. DOI
48. Shao, L.; Sang, Y.; Liu, N.; et al. Selectable microporous carbons derived from poplar wood by three preparation routes for CO_2 capture. *ACS. Omega.* **2020**, *5*, 17450-62. DOI PubMed PMC
49. Shao, L.; Liu, M.; Sang, Y.; Zhan, P.; Chen, J.; Huang, J. Nitrogen-doped ultrahigh microporous carbons derived from two nitrogen-containing post-cross-linked polymers for efficient CO_2 capture. *J. Chem. Eng. Data.* **2020**, *65*, 2238-50. DOI
50. Yang, K.; Yang, Z.; Zhang, C.; et al. Recent advances in CdS-based photocatalysts for CO_2 photocatalytic conversion. *Chem. Eng. J.* **2021**, *418*, 129344. DOI
51. Shen, Y.; Zheng, Q.; Zhu, H.; Tu, T. Hierarchical porous organometallic polymers fabricated by direct knitting: recyclable single-site catalysts with enhanced activity. *Adv. Mater.* **2020**, *32*, e1905950. DOI PubMed
52. Wen, D.; Zheng, Q.; Yang, S.; Zhu, H.; Tu, T. Direct knitting boosts the stability and catalytic activity of NHC-Au complexes towards valorization of SO_2 and CO_2. *J. Catal.* **2023**, *418*, 64-9. DOI
53. Nunes, P.; Correia, I.; Marques, F.; et al. Copper complexes with 1,10-phenanthroline derivatives: underlying factors affecting their cytotoxicity. *Inorg. Chem.* **2020**, *59*, 9116-34. DOI PubMed
54. Pu, Y.; Harding, R. E.; Stevenson, S. G.; et al. Solution processable phosphorescent rhenium(i) dendrimers. *J. Mater. Chem.* **2007**, *17*, 4255-64. DOI
55. Ge, Z.; Hayakawa, T.; Ando, S.; et al. Synthesis and properties of 3,8-Bis[4-(9*H*-carbazol-9-yl)phenyl]-1,10-phenanthroline for phosphorescent OLEDs. *Chem. Lett.* **2008**, *37*, 262-3. DOI
56. Chen, J.; Li, H.; Zhong, M.; Yang, Q. Hierarchical mesoporous organic polymer with an intercalated metal complex for the efficient synthesis of cyclic carbonates from flue gas. *Green. Chem.* **2016**, *18*, 6493-500. DOI
57. Li, H.; Feng, X.; Shao, P.; et al. Synthesis of covalent organic frameworks *via in situ* salen skeleton formation for catalytic applications. *J. Mater. Chem. A.* **2019**, *7*, 5482-92. DOI
58. Chen, J.; Zhong, M.; Tao, L.; et al. The cooperation of porphyrin-based porous polymer and thermal-responsive ionic liquid for efficient CO_2 cycloaddition reaction. *Green. Chem.* **2018**, *20*, 903-11. DOI
59. Ouyang, H.; Song, K.; Du, J.; Zhan, Z.; Tan, B. Creating chemisorption sites for enhanced CO_2 chemical conversion activity through amine modification of metalloporphyrin-based hypercrosslinked polymers. *Chem. Eng. J.* **2022**, *431*, 134326. DOI
60. Dong, Y.; Liu, H.; Wang, S.; Guan, G.; Yang, Q. Immobilizing isatin-schiff base complexes in NH_2 -UiO-66 for highly photocatalytic CO_2 reduction. *ACS. Catal.* **2023**, *13*, 2547-54. DOI
61. Cui, J.; Fu, Y.; Meng, B.; et al. A novel cobalt-anchored covalent organic framework for photocatalytic conversion of CO_2 into widely adjustable syngas. *J. Mater. Chem. A.* **2022**, *10*, 13418-27. DOI
62. Yang, Y.; Lu, Y.; Zhang, H.; et al. Decoration of active sites in covalent-organic framework: an effective strategy of building efficient photocatalysis for CO_2 reduction. *ACS. Sustain. Chem. Eng.* **2021**, *9*, 13376-84. DOI
63. Zhong, W.; Sa, R.; Li, L.; et al. A covalent organic framework bearing single Ni sites as a synergistic photocatalyst for selective photoreduction of CO_2 to CO. *J. Am. Chem. Soc.* **2019**, *141*, 7615-21. DOI PubMed
64. Han, B.; Ou, X.; Zhong, Z.; Liang, S.; Deng, H.; Lin, Z. Rational design of FeNi bimetal modified covalent organic frameworks for photoconversion of anthropogenic CO_2 into widely tunable syngas. *Small* **2020**, *16*, e2002985. DOI PubMed

65. Hu, X.; Zheng, L.; Wang, S.; Wang, X.; Tan, B. Integrating single Co sites into crystalline covalent triazine frameworks for photoreduction of CO_2. *Chem. Commun.* **2022**, *58*, 8121-4. DOI PubMed